JOINT STATISTICS OF SOOT VOLUME FRACTION, PRIMARY PARTICLE DIAMETER AND TEMPERATURE IN FLAMES. PART II: VALUE OF QUANTITATIVE PLANAR MEASUREMENTS OF MULTIPLE PARAMETERS

Zhiwei Sun[1,2,*], Zeyad Alwahabi[1,3], Bassam Dally[1,2], Graham Nathan[1,2]
[*]email: zhiwei.sun@adelaide.edu.au
[1]Centre for Energy Technology (CET), [2]School of Mechanical Engineering, and [3]School of Chemical Engineering, The University of Adelaide, SA 5005, Australia

Abstract
In our previous paper, an optical setup used for simultaneous, planar and quantitative measurements of soot volume fraction (f_v), primary particle diameter (d_p) and flame temperature (T) in sooting flames was introduced [1]. The details of the optical setup that combines non-linear two-line atomic fluorescence (nTLAF) and time-resolved laser-induced incandescence (TiRe-LII) have been presented, together with accuracy and precision assessments. This paper, as **Part II** of the work, presents the value of the quantitative planar measurements that are uniquely achieved using the setup. The advantages include corrections for local, instantaneous flame temperature in the planar TiRe-LII for d_p imaging and the capabilities of accessing the gradients of the key parameters and their distributions in the direction relative to local soot sheet structures.

1. Introduction
Significant efforts have been made to develop instantaneous, two dimensional laser diagnostic techniques that are used for turbulent flames [1]. Using these optical tools with high spatial and temporal resolutions, detailed flame structures and their changes in time and space are visualized. These optical methods become extremely significant when quantitative results are accessible using them. However, most previous work of quantitative measurement generally presented the results that are also accessible through point- or line-wise measurements. This is also true in the measurements of turbulent sooting flames using planar quantitative techniques. Most previous results are the mean values of the measured parameters together with the corresponding RMS along the flame axial or radial direction, as well as their joint probability density function ($jPDF$), e.g. [2, 3, 4]. While these quantitative results are necessarily important in validating soot models, it is also highly desirable to extract information that is relative to the flame structures in these diffusion flames, such as the distribution of a measured parameter along the direction normal to soot sheets. These quantitative information is equally important as those along axial or radial direction in the Eularian coordinate system. However, this kind of assessment has not been widely performed neither in turbulent sooting flames maybe because the significance of such an assessment becomes for qualitative measurements, nor in premixed flames maybe because such information is not important when diffusion is not a dominate controlling factor. Simultaneous and quantitative imaging soot volume fraction (f_v), primary particle diameter (d_p) and flame temperature (T) were achieved using our nTLAF+TiRe-LII setup [2, 5, 6]. This provides opportunities to conduct such an assessment to extract more quantitative information relative to flame detailed structures or the intermittent soot sheets. Therefore, it is desirable to develop a methodology to extract

[1]Also presented at this conference and entitled: Joint statistics of soot volume fraction, primary particle diameter and temperature in flames. Part I: Experimental setup.

such spatial relationships between f_v, T and d_p in local coordinator that is relative to flame structures. This can also double the value of the developed planar diagnostic techniques.

In addition, simultaneous measurement of multi- key parameters also benefits the accuracy of the results. The TiRe-LII technique that is used for d_p measurements in the present work is relevant to flame temperature T, i.e. the decay of LII signals is dependent on flame temperature in addition to d_p. Sun et al. demonstrated single-shot imaging of d_p in unsteady premixed flames using planar TiRe-LII [7] and showed that d_p is very sensitive to local flame conditions. Cenker et al. performed two-time-step LII to image d_p in a high-pressure diesel combustion vessel and compared the results with those obtained from thermophoretic sampling [8]. Their accompanying sensitivity analysis suggested that the accurate calculation of d_p from these parameters should employ a local flame temperature measured simultaneously as an input to the model [9]. This is also a point discussed and identified elsewhere [10, 11]. Hadef et al. incorporated flame temperature information, which was obtained from non-simultaneous coherent anti-Stokes Raman spectroscopy (CARS) measurements, in a gated TiRe-LII measurement [10]. However, no quantitative assessment of this correction is available in turbulent flames, even for point-wise TiRe-LII, since this requires simultaneous measurement of flame temperature. There is, therefore, a need to quantify the significance of the correction of TiRe-LII for local gas temperature simultaneously measured.

In light of the above background, the specific aims of the present investigation are (1) to assess the efficacy of a correction for local, instantaneous flame temperature in the planar TiRe-LII; and (2) to develop an methodology to extract detailed relationships between the measured parameters along the direction normal to the principal orientation of local soot sheets.

2. Experiment

Results presented in this work are measured in the same experiment campaign using the upgraded nTLAF+TiRe-LII setup, as described in Part I [6]. Measurements were conducted in an unsteady, wrinkled flame burning a mixture of ethylene (2.211 standard liters per minutes, SLM) and air (1.0 SLM), stabilized on the same burner as described in Part I [6]. The fuel jet Reynolds number (Re) is 641, while the flow rate of co-flowing air is 43 SLM.

Part of the results for a steady ethylene/air diffusion flame are also presented to enable a comparison with those in the unsteady flame. Details of the steady and the results can be found in *Part I* of this work [6]. The flame is a Santoro-type flame with a luminous height of $\sim$ 64 mm.

3. Results and discussion

3.1 Simultaneous images and joint PDFs

Figure 1 presents typical simultaneous images of T, f_v and d_p in the unsteady laminar flame. The measured flame temperatures were taken into account in the evaluation of d_p. While not truly turbulent, this condition generates relatively large-scale vortices that wrinkle the flame to generate convex and concave strain that is easier to interpret than in turbulent flames. Figure 1 reveals that flame temperature is distributed over a much wider range than in the steady flames. Particularly in Figs. 1*d*, *f*, *g* and *i*, the temperature is even approaching to 2800 K in non-sooting regions, which may be not acceptable because the adiabatic temperature for ethylene/air flame is 2391 K when equivalence ratio is 1.1. Noting these unexpected temperature values are not found in the steady flame measured in the same experiment campaign [6], they should be relevant to the unsteadiness of the flame flow. Figure 1 also reveals that the measurements are consistent with the expected trend of

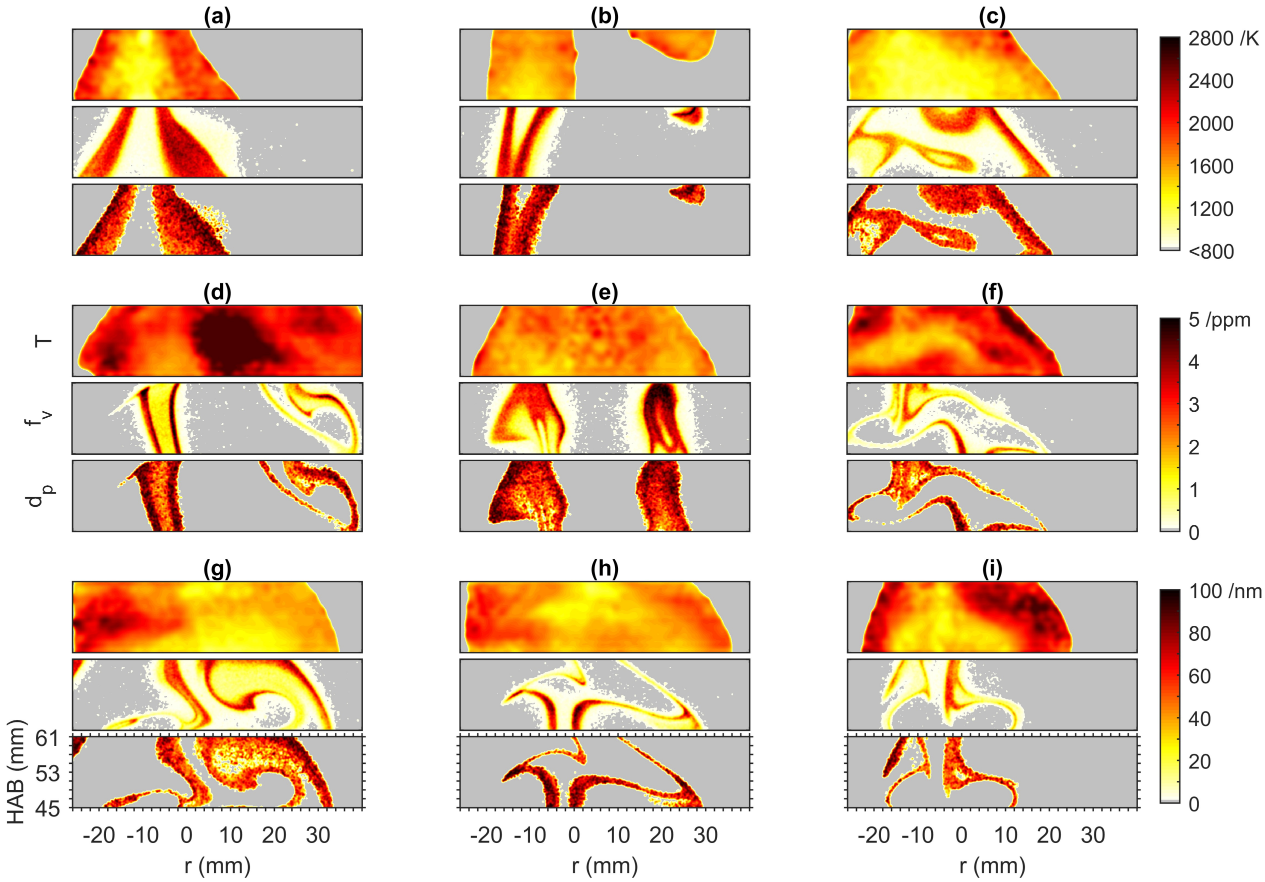

Figure 1: Examples of single-shot, simultaneous images of T, f_v and d_p in the unsteady sooting flame (Re = 641).

soot found in the steady laminar flame [6], in which soot sheets are generally found in the relatively low temperature regions on the rich side of the high temperature reaction zone. However, the relationship is more complex than this. It can be seen from Fig. 1d that, in addition to the generally good correlation between f_v and d_p, there is an additional trend in which d_p increases with axial distance. While f_v tends to peak near to the middle of a given soot sheet, d_p tends to grow with axial distance and peak near to the oxidation side of a soot sheet. The complex relationships between these parameters demonstrate the need for application of the method, together with the use of statistical analysis, in parallel with computational modeling, to provide more detailed explanations.

3.2 Temperature correction for d_p measurement

Figure 2 presents a typical image of the difference between d_p as determined using either a measured temperature or an constant temperature of 1700 K. While the influence of such an assumption of a constant temperature is negligible in the steady flame as soot distributes in a narrow temperature range around 1700 K), in the unsteady flame it can result in a ±10% uncertainty in the single-shot d_p imaging. This is because soot distributes within a wider temperature range when the flame is unsteady (see $jPDF$ in section 3.3). As shown in Fig. 2, at (r, HAB) = (30 mm, 57 mm) an underestimation of the flame temperature results in overestimation of d_p values and vice versa, notably at (r, HAB) = (-2 mm, 47 mm). Considering the relatively low precision of d_p at ±20% (see Figure 6 in Part I [6]), this

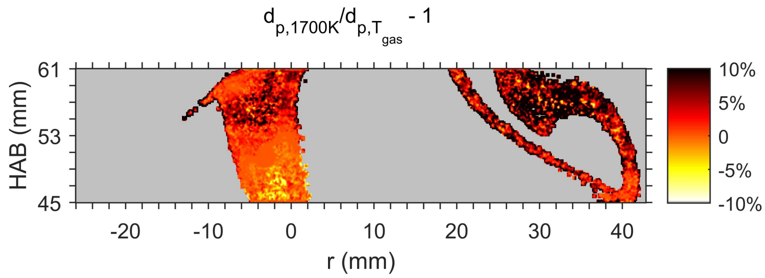

Figure 2: A typical image of the difference between d_p as determined using either a measured temperature or an constant temperature of 1700 K. This image is corresponding to Fig.1d.

additional uncertainty ($\pm 10\%$) is second order. Nevertheless, in highly turbulent flames or other combustion conditions (e.g. oxygen enriched sooting flames that we have investigated recently) where soot distributes over a much wider temperature range [12], it can become increasingly important. In addition, the ongoing development of imaging devices will make the use of this correction increasingly important as cameras with reduced noise become available.

3.3 Value of quantitative planar measurements

This section presents some results that are not accessible from point- or line-wise measurements but can be derived from planar measurements. Also presented is a method for extracting statistical data based on local coordinates that move with the soot sheet, rather than being fixed in space as occurs with a conventional Eularian frame of reference.

A direct benefit from planar measurement is that it allows gradients to be derived. Figure 3 presents typical images of the values of f_v and d_p together with their spatial gradients. To the best of our knowledge, these represent the first time such gradients of d_p have been reported, since these data can only be derived from single-shot planar measurements with sufficiently good signal-to-noise ratio. Instantaneous temperature fields are more flat in diffusion flames than in premixed ones, so that we have not presented images of temperature gradients. From the derived gradient images, statistics relative to $|\nabla f_v|$ and $|\nabla d_p|$ can be calculated, e.g. the mean values and the RMS along the flame centreline or their radial profiles, as well as single or joint $PDFs$. Also noted is that only quantitative measurements as conducted in the present work make such images of gradients accessible.

It can be seen in Fig. 3 that strong gradients in both f_v and d_p occur at the outer edges of the soot sheet structures, where high values of the original parameters also occur. However, the locations of peak gradients are not necessarily well correlated with the locations of the maximum values of the original parameters and can even be anti-correlated. High values of f_v are generally found throughout the upper region of this flamelet, where the corresponding gradients are low. Similarly, the values of d_p tend to increase with axial distance in this image, so that the gradients are high in the lower part of the flamelet, but not in the upper region.

Figure 4 presents the $jPDF$ between f_v and T and that between f_v and d_p in the steady and unsteady flames. For the steady flame, these statistics were calculated over the entire flame from the averaged images (see images presented in part I [6]), while for the unsteady flame they are calculated over the entire flame width between HAB = 45 and 61 mm from 100 single-shot images. Such statistics provides significantly valuable information to understand the sooting flames. It can be seen that the soot in the unsteady flame is distributed over a

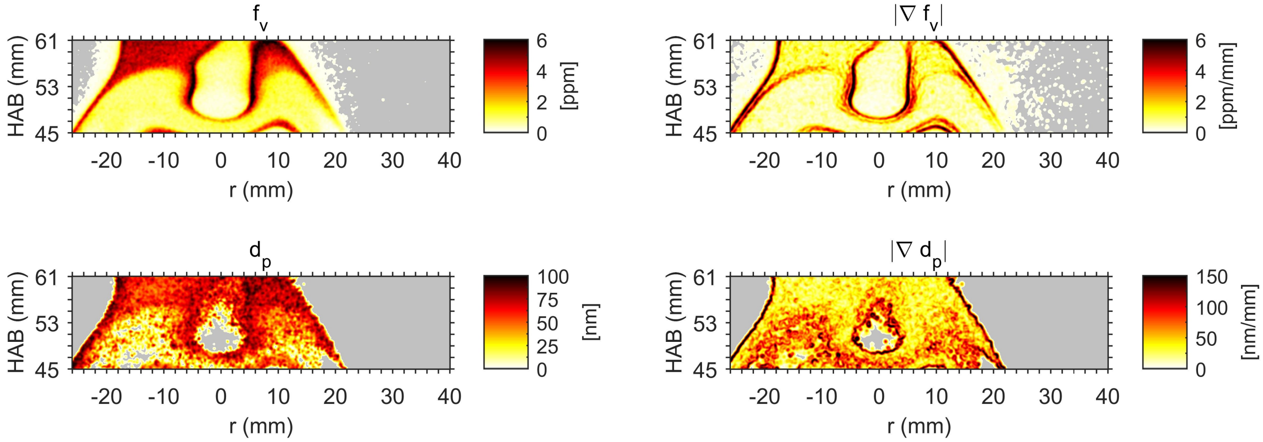

Figure 3: Representative images of f_v and d_p measured in the unsteady flame and their corresponding gradients.

much wider range of temperatures than in the steady flame. In addition, despite similarities in the broad distribution of the $jPDF$ of f_v and d_p, the peak values are found toward the edge of the envelope for the steady flame and in the middle for the unsteady flame. Nevertheless, despite the value of these data, they are limited by the Eulerian frame of reference. Particularly for the unsteady case, it is not possible to relate these statistics to their position relative to the local reaction zone, which fluctuates both in time and space. As each planar image also contains additional information about the instantaneous position of the local reaction zone, a methodology has also been developed to extract data based on the local coordinates of the instantaneous flame structure. This method, which is illustrated in Figure 5, comprises the following steps:

1. Determine a local coordinate that can be used to characterise the primary orientation of a soot sheet. Here we report the case based on a threshold of 1 ppm, which occurs on both sides of soot sheets of sufficiently high local volume fraction due to its relative simplicity. However, we are also evaluating other criteria based on gradient methods and maximum values of f_v. This local coordinate is called x'.

2. Extract data based on the local coordinate normal to the orientation of the principal orientation, here termed r'. So that $r' = 0$ is on the principal local coordinate. While the method could be applied statistically for all data (x'), here we only report data for selected points. These selected x' can either equally distributed in local coordinate x' (i.e. along the determined soot edge [13]) or equally distributed in space in the Eulerian frame. The latter selection was used in the present work.

3. The *positive* direction of the normal coordinate r' is defined as the direction of *walking into* the soot sheet, i.e. following $\frac{df_v}{dr'} \geq 0$.

4. Determine whether the side of the soot sheet is within the oxidising or reducing side of the reaction zone, based on the local temperature gradient. That is, the oxidising side r'_{ox} is conditional on $\frac{dT}{dr'} < 0$, while r'_{red} is conditional on $\frac{dT}{dr'} \geq 0$.

Figure 6 presents the profiles of f_v, d_p and T based on the local coordinates for the steady and unsteady flames. These images highlight the value of extracting data based on local coordinates. In contrast to the Eularian statistics (Figure 4), far these data confirm

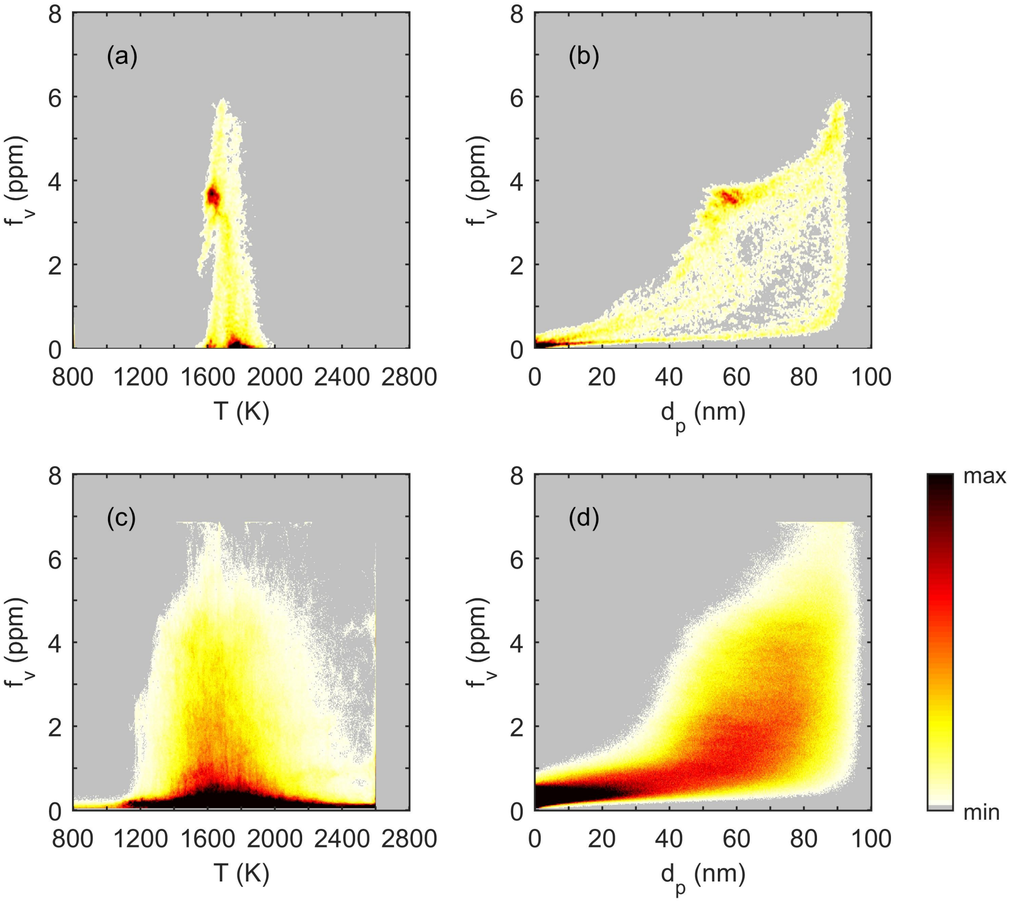

Figure 4: (**a** and **b**) Joint PDFs between f_v and T and that between f_v and d_p in the steady flame calculated over the whole flame region as shown in Figure 3 in Part I [6], and (**c** and **d**) that in the unsteady flame calculated for the measured region as shown in Fig. 1 over 100 images.

that the combustion is operating within the wrinkled laminar flamelet regime. That is, the local distributions of T, f_v and d_p are quite similar for the unsteady and steady flames, although the distributions for the unsteady cases are generally broader than those of the steady flames. Similarly, the profiles on the oxidising and reducing sides of the flames are also broadly similar, although exhibiting differences. Calculations from a larger data set is required to better quantify the extent of the differences and to extend the method into the turbulent flame regime. Moreover, in our work followed, simultaneous planar LIF of hydroxyl (OH) is involved to identify the oxidation region, replacing the use of the temperature profile.

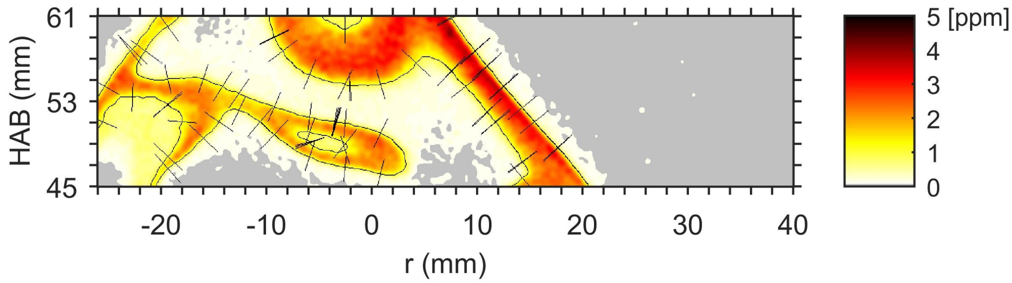

Figure 5: A typical image of f_v, superimposed with a series of local coordinates of r' that are oriented normal to the primary coordinate aligned with the soot sheet, derived here from thresholding at 1 ppm.

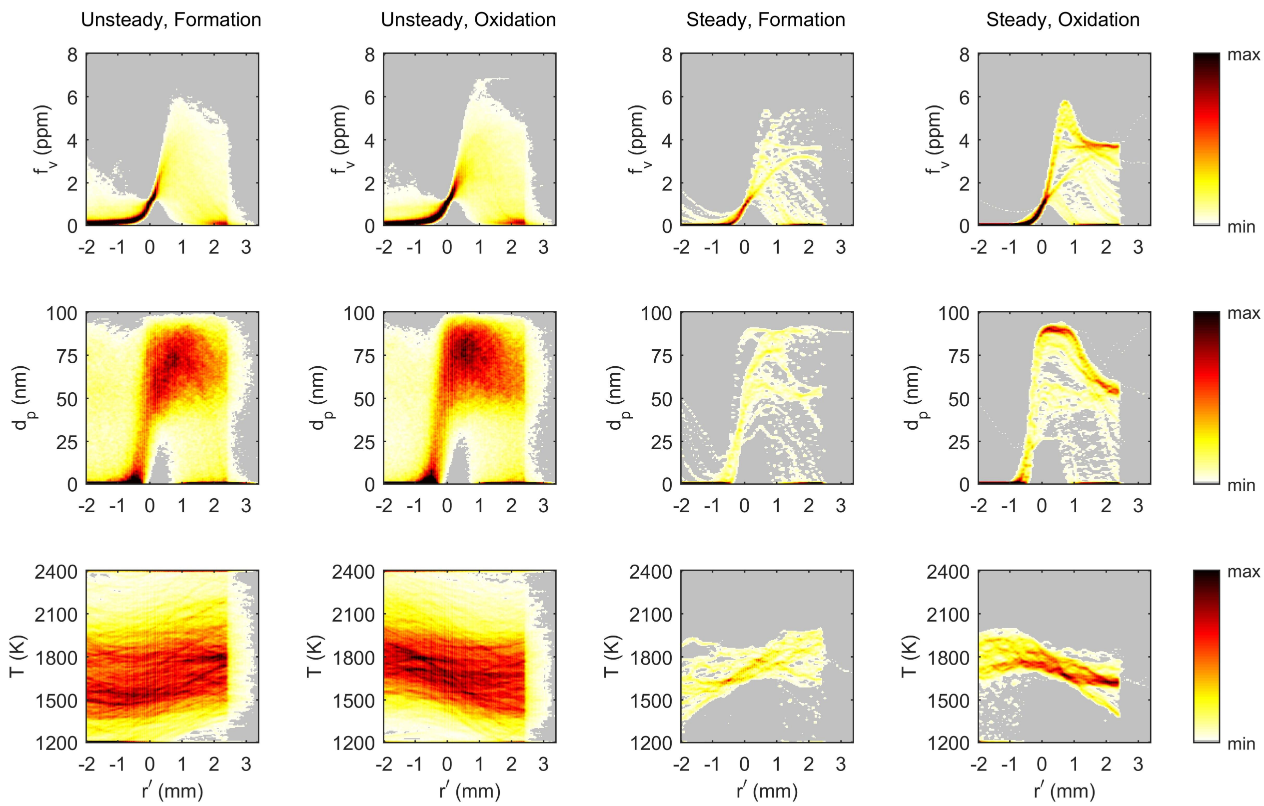

Figure 6: Profiles of f_v, d_p and T derived fro the local coordinates for the unsteady (the left two) and the steady flames (the right two). The profiles are further categorised as being on the formation or oxidising sides of the soot sheets based on their corresponding temperature profiles.

4. Conclusions

The benefit of correcting the values of d_p with the measured flame temperature is $\sim$10% in the unsteady laminar flame, which is relatively small compared with the precision of d_p measurement ($\sim$20%) using currently available imaging technology. Nevertheless, the significance of this correction may increase with the degree of unsteadiness in the flame (which will increase the range of temperatures at which soot is found) and with the ongoing advances in the planar TiRe-LII method.

A method of deriving profiles through soot sheets that are referenced to a local, unsteady coordinate system was presented. This reveals that local sheets behave as wrinkled laminar flamelets with a similar, but broader distribution. These results demonstrate the value of quantitative, simultaneous planar imaging techniques. Together these measurements have enabled the first measurements of transects through wrinkled flamelets that are based on coordinates tied to the local fluctuating flame-front, rather than to coordinates fixed in space. Future work will add the position of OH-PLIF, which has recently been integrated into our optical system.

Acknowledgments
The Australia Research Council is gratefully acknowledged for financial support (DP130100198). The authors thank Dr. Dahe Gu and Mr. KaeKen Foo for their assistance in the experiment.

References

[1] Aldén, M., Bood, J., Li, Z., Richter, M., "Visualization and understanding of combustion processes using spatially and temporally resolved laser diagnostic techniques", *Proceedings of the Combustion Institute* 33:69 – 97 (2011).

[2] Gu, D., Sun, Z., Dally, B.B., Medwell, P.R., Alwahabi, Z.T., Nathan, G.J., "Simultaneous measurements of gas temperature, soot volume fraction and primary particle diameter in a sooting lifted turbulent ethylene/air non-premixed flame", *Combustion and Flame* 179:33 – 50 (2017).

[3] Köhler, M., Geigle, K.P., Blacha, T., Gerlinger, P., Meier, W., "Experimental characterization and numerical simulation of a sooting lifted turbulent jet diffusion flame", *Combustion and Flame* 159:2620–2635 (2012).

[4] Park, O., Burns, R.A., Buxton, O.R., Clemens, N.T., "Mixture fraction, soot volume fraction, and velocity imaging in the soot-inception region of a turbulent non-premixed jet flame", *Proceedings of the Combustion Institute* 36:899 – 907 (2017).

[5] Foo, K.K., Sun, Z., Medwell, P.R., Alwahabi, Z.T., Dally, B.B., Nathan, G.J., "Experimental investigation of acoustic forcing on temperature, soot volume fraction and primary particle diameter in non-premixed laminar flames", *Combustion and Flame* 181:270 – 282 (2017).

[6] Zhiwei Sun, Bassam Dally, Z.A., Nathan, G., "Joint statistics of soot volume fraction, primary particle diameter and temperature in flames. part i: Experimental setup", *The Mediterranean Combustion Symposium* 10 (2017).

[7] Sun, Z.W., Gu, D.H., Nathan, G.J., Alwahabi, Z.T., Dally, B.B., "Single-shot, time-resolved planar laser-induced incandescence (tire-lii) for soot primary particle sizing in flames", *Proceedings of the Combustion Institute* 35:3673–3680 (2015).

[8] Cenker, E., Kondo, K., Bruneaux, G., Dreier, T., Aizawa, T., Schulz, C., "Assessment of soot particle-size imaging with lii at diesel engine conditions", *Appl. Phys. B* 119:765–776 (2015).

[9] Cenker, E., Bruneaux, G., Dreier, T., Schulz, C., "Sensitivity analysis for soot particle size imaging with laser-induced incandescence at high pressure", *Appl. Phys. B* pp. 1–19 (2015).

[10] Hadef, R., Geigle, K., Zerbs, J., Sawchuk, R., Snelling, D., "The concept of 2d gated imaging for particle sizing in a laminar diffusion flame", *Appl. Phys. B* 112:395–408 (2013).

[11] Schraml, S., Dankers, S., Bader, K., Will, S., Leipertz, A., "Soot temperature measurements and implications for time-resolved laser-induced incandescence (tire-lii)", *Combustion and Flame* 120:439–450 (2000).

[12] Chan, Q.N., Medwell, P.R., Kalt, P.A.M., Alwahabi, Z.T., Dally, B.B., Nathan, G.J., "Simultaneous imaging of temperature and soot volume fraction", *Proceedings of the Combustion Institute* 33:791–798 (2011).

[13] Kamal, M.M., Coriton, B., Zhou, R., Frank, J.H., Hochgreb, S., "Scalar dissipation rate and scales in swirling turbulent premixed flames", *Proceedings of the Combustion Institute* 36:1957 – 1965 (2017).